Hindawi
Mathematical Problems in Engineering
Volume 2020, Article ID 3206864, 18 pages
https://doi.org/10.1155/2020/3206864

Research Article

Robust Feedback Control for Nonminimum Phase, Delayed, or Unstable Systems with Multiple Inputs

Montserrat Gil-Martínez and Javier Rico-Azagra

Electrical Engineering Department, University of La Rioja, Logroño, Spain

Correspondence should be addressed to Javier Rico-Azagra; javier.rico@unirioja.es

Received 11 October 2019; Revised 13 January 2020; Accepted 10 February 2020; Published 4 April 2020

Academic Editor: Libor Pekař

This paper presents a feedback control solution that achieves robust stability and disturbance rejection in systems with multiple manipulated inputs and a single measurable output. The uncertain plant models may exhibit either nonminimum phase, or delay, or unstable phenomena, which makes it not easy to take full advantage of the frequency response of each plant. In the framework of quantitative feedback theory (QFT), a methodology is proposed to decide the best control bandwidth distribution among inputs and to design the set of parallel controllers with as small as possible gain at each frequency. The temperature regulation in a continuous stirred-tank reactor (CSTR) illustrates the benefits of a quantitative frequency distribution of the dynamic controllability between the jacket flow and the feed flow. The main challenge is that the feed flow exhibits a higher temperature regulation capacity and also produces a temporary decrease in the reactor temperature (nonminimum phase behaviour).

1. Introduction

The collaboration of multiple inputs at a time to regulate a single measurable output (MISO control) is often considered in process control to increase control authority, performance, or flexibility. How to use the additional degrees of freedom has led to different designations, structures, and design methods in the scientific literature. On the basis of the inputs differing significantly in their dynamic effect on the output and the relative cost of manipulating each one, *valve position control* [1] and *habituating control* [2] pursue the participation of each input along different frequency bands. Thus, a chained intervention of gradually slower loops takes place whenever the output is deviated from its set point. This also makes the slowest inputs reset the fastest inputs (*input resetting control* [3]) to convenient set points (*midranging control* [4]), which prevents the saturation of actuators and may report economical benefits in different ways. For example, since the cheapest input manages the stationary [2, 5], or since the midrange set points condition a more profitable equilibria of the whole set of manipulated inputs [6, 7]. A serial arrangement of feedback controllers [2, 8] offers a more transparent design methodology in accordance with the previous objectives. Alternatively, a parallel arrangement (Figure 1) is more general and flexible [2]. In fact, it provides the ability of several inputs collaborating along the same frequency band [9], and eventually, the control bandwidth distribution among the inputs as desired [10]. It is also common to separate a master centralised controller from the parallel structure of branch elements [11] (slaves), as in *load-sharing* applications [12]. This paves the way to much more complex distribution structures [13] and specific algorithms among which the model predictive control and optimization techniques are frequent [2, 4, 9]. In general, it can be regarded as a hierarchical structure where the high-level linear controller faces the single output regulation by yielding a single virtual control input. Then, a low-level *control allocation* algorithm coordinates the different manipulated inputs such that they together produce the desired virtual control effort, if possible [14]. Nonlinear approaches to control allocation are common in flight control, marine applications, automotive, and other industries where mechatronics prevails [15, 16]. Optimization-based allocation methods are referred in [17]. The relevance of different

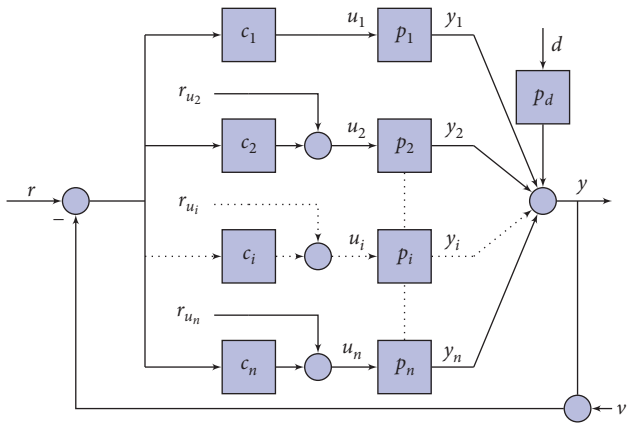

Figure 1: Parallel control structure for MISO systems.

multi-input control approaches is supported by recent applications in several fields such as process control [7, 18, 19], medical systems [20–22], robotics [23–25], unmanned aerial vehicles [26, 27], automotive industry [28], and electrical power systems [29].

Nonminimum phase (NMP) behaviours (or delays) are frequent in MISO process control. The design methods in [1, 2, 30] pay special attention to them inside serial arrangements of controllers. Those strategies make the inputs collaborate over different bands of frequency, such that the NMP input handles the low-frequency band and does not limit the achievable performance. However, as long as the inputs cannot collaborate along the same frequencies, a control effort reduction is not possible by using redundant control inputs. On the other hand, authors in [9, 11] present methods for some kind of parallel structure, which allows a potential collaboration of inputs over the same frequencies. Alvarez-Ramirez et al. [9] illustrate how less-expensive control effort can be obtained with the addition of redundant control inputs, but such a cost saving is obtained at the expense of a sluggish closed-loop response if any additional control input is of the NMP nature. Thus, the drawback of the method is that the inputs are forced to collaborate along the same frequency band. Schroeck et al. [11] propose a master-slaves structure and develop a *PQ method* for control design. Firstly, the slaves are designed bearing in mind the following issues: (a) they condition the zeros of the equivalent slaves-plants avoiding that they are located in the right half-plane (RHP) and may limit the achievable closed-loop performance; (b) they determine the relative magnitude contribution to the output (a separated contribution of the inputs along the frequency band is pursued); (c) the relative phase contribution may be critical if they are out of phase when their magnitude contribution is nearly the same (destructive interference). Secondly, the master achieves the desired performance and stability. The PQ method has been proved in a hard disk drive application [11] and in a turbocharged engine control [31]. Some drawbacks of the method are the inputs eventually collaborate in different frequencies, the slaves are designed open loop with no reference to the closed-loop specifications, which can negatively interfere with the master task, and the control structure and the design method are complex when the number of inputs grows. Finally, any specific method in the scientific literature has dealt with the potential collaboration of unstable systems to the best of the author's knowledge.

The frequency domain appears to be the most meaningful approach to determine the best input participation, under the assumption that the system can be approximated by linear models. And, the parallel structure in Figure 1 is being used to freely distribute the frequency band. A proper scaling of all u_i input ranges allows fairer comparisons as it considers saturation constraints. Then, the frequency response (y/u_i), i.e., $p_i(j\omega)$, reveals the relative "capacity" of each input; p_i plant models can include uncertainty, for example, corresponding to unmodelled dynamics or small-signal linear approximations of nonlinearities. The capacity of each $p_i(j\omega)$ plant is in reference to the closed-loop bandwidth (required performance). Inside the framework of quantitative feedback theory (QFT), the bounds express, at discrete frequencies, the set of closed-loop specifications in terms of the nominal open-loop transfer function, which initially matches the nominal plant [32, 33]. In this way, special bounds [10] depict in a transparent and quantitative way the capacity of each plant of the MISO system to achieve the specifications. A comparison of those bounds helped to distribute the control bandwidth among loops in order to get the set of controllers of minimum gain at each frequency [10]. Several inputs could either collaborate at a certain frequency to reduce the individual control effort or be inhibited to avoid useless fatigue and saturation risk of actuators. However, only magnitude contributions of plants (inputs) were taken into account, which only works well for minimum-phase (MP) plants. This paper develops a method that takes into account the relative phase of the branches under the potential presence of RHP dynamics (zeros or poles) or delays. If branches were out of phase, they would fight each other and the total output magnitude would drop considerably .

The paper is organised as follows: Section 2 formulates the feedback control problem to be solved inside a QFT framework. Then, it puts forward the challenges to decide the best control bandwidth distribution when output/input relations are not in the minimum phase; in particular, the unstable case is analysed by an example. Finally, the section summarises the methodology to find the set controllers of smallest gain at each frequency. Section 3 applies it for the dual-input control of a continuous stirred-tank reactor (CSTR), where a convenient distribution of feedback improves the system controllability despite the nonminimum phase behaviour of one manipulated input. Conclusions are in Section 4.

2. MISO Control to Reduce the Feedback Demand

2.1. Statement of the Robust Regulation Problem. Figure 1 depicts an architecture of n parallel feedback controllers $c_{i=1,\ldots,n}(s)$. Each plant $p_i(s)$ models the dynamic response from the manipulated input u_i to the single controlled

output y. The plant $p_d(s)$ determines how a nonmeasurable disturbance d deviates the output y from its set point r. Each actuator contribution in the steady state can be conveniently selected by set points r_{u_i} for $n-1$ manipulated inputs at most. At least a plant (i.e., p_1) will work in the low-frequency band, and $u_{i=1}$ will compensate any output deviation in steady state. External input v represents the high-frequency noise associated with the single sensor that measures the output y.

Uncertainty of plant models is being explicitly considered in the collaborative control design. Thus, let us take a $1 \times (n+1)$ vector of plant transfer functions $\mathbf{P} = [p_{i=1,\ldots,n}, p_d]$, which can be any element of

$$\mathscr{P} = \left\{\mathbf{P}\left(s, \mathbf{q}_j\right) : \mathbf{q}_j \in \mathscr{Q}\right\}, \tag{1}$$

where $\mathbf{q}_j$ is a vector with the m uncertain parameters of plant models and $\mathscr{Q}$ is the set in $\mathbb{R}^m$ that is defined by all its possible values.

Then, if a certain performance model is desired for d disturbance rejection at the y output, QFT defines the robust specification in the frequency domain $s = j\omega$, $\omega = [0, \infty)$ as

$$\left|T_d(j\omega)\right| = \left|\frac{y(j\omega)}{d(j\omega)}\right| = \left|\frac{p_d(j\omega)}{1 + l_t(j\omega)}\right| \le \left|W_d(j\omega)\right|; \quad \forall \mathbf{P}(j\omega), \forall\omega, \tag{2}$$

where $l_t = \sum_{i=1}^{n} l_i$ denotes the total open-loop transfer function that is contributed by branches $l_i = p_i c_i$. Additionally, occasional changes in r_{u_i} may be of interest, and robust specifications on (y/r_{u_i}) responses can be also taken into account. From a mathematical point of view, these can be treated identically to (2). Thus, they are here being omitted for simplicity.

Robust stability in $s = j\omega$, $\omega = [0, \infty)$ is being defined by the set

$$\left|T_i(j\omega)\right| = \left|\frac{\left(l_i(j\omega)/\left(1 + \sum_{j\neq i} l_j(j\omega)\right)\right)}{\left(1 + l_i(j\omega)/\left(1 + \sum_{j\neq i} l_j(j\omega)\right)\right)}\right| = \left|\frac{l_i(j\omega)}{1 + l_t(j\omega)}\right| \le W_{s_i}, \quad i = 1, \ldots, n; \ \forall \mathbf{P}(j\omega), \forall\omega, \tag{3}$$

where the upper tolerance W_{s_i} means the minimum distance from $(l_i(j\omega)/(1 + \sum_{j\neq i} l_j(j\omega)))$ to the critical point -1. It is usually of interest to assure a certain phase margin PM_i by taking

$$W_{s_i} = \frac{1}{2\sin\left(\mathrm{PM}_i/2\right)}, \tag{4}$$

or, if preferred, to choose a certain gain margin GM_i by taking

$$W_{s_i} = \frac{1}{\mathrm{GM}_i - 1}, \quad \mathrm{GM}_i > 1. \tag{5}$$

Robust stability (3) is straight forward related to individual loops, while robust performance (2) is a collaborative task among loops.

The $c_i$controller design is being executed by loop-shaping a nominal open-loop $l_{o_i}(j\omega) = p_{o_i}(j\omega)c_i(\omega)$ on a mod-arg chart. $l_{o_i}(j\omega)$ has to meet the QFT bounds $\beta_{l_i}(\omega)$, which are computed at discrete frequencies $\omega \in \Omega$. These β_{l_i}-bounds translate the closed-loop robust specifications (2)–(3) in terms of l_{o_i}, and they can be computed by using the command *genbnds* of Terasoft QFT Toolbox [34]. It handles specifications in the general form:

$$\left|\frac{A + BG}{C + DG}\right| \le |W|, \tag{6}$$

where G is the c_i-controller to be designed and functions A, B, C, D, and W can be easily identified by comparison with (2)–(3).

The aim is obtaining the feedback control solution $c_{i=1,\ldots,n}$ that achieves (2)–(3) using as small as possible control gain at each frequency. The challenge is how to distribute the collaborative task over the frequency band among loops despite the fact that plants $p_{i,\ldots,n}$ contain RHP poles, RHP zeros, or delays.

2.2. Challenges in the Collaboration of Plants with RHP Dynamics. Let us suppose a system where two inputs can intervene in the output regulation. The uncertainty-free plant models are

$$p_1(s) = \frac{1}{s+1}, \qquad p_2(s) = \frac{1}{s-1}, \qquad p_d(s) = 1. \tag{7}$$

The disturbance rejection model

$$W_d(s) = \frac{1.75s}{(s+12)}, \tag{8}$$

defines the desired (y/d) behavior (2). For a minimum phase margin of 40° at both loops (3), the tolerance choice (4) is

$$W_{s_{i=1,2}} = 1.462. \tag{9}$$

QFT bounds will represent those closed-loop specifications in terms of open-loop transfer functions at the discrete set of ω-frequencies:

$$\Omega = \{0.1, 0.3, 1, 2, 3, 6, 10, 20, 50\}\,[\mathrm{rad}/s]. \tag{10}$$

In order to compare the capacity of each plant in the regulation task, let us firstly solve the problem assuming that only one of the two plants (inputs) participates at a time. For the case of p_1 alone participation, the bounds β_{l_1} in Figure 2(a) show the feedback demand in terms of $l_t = l_1$. The initial location of this open-loop function is p_1 since $c_1 = 1$. A possible solution $l_1 = p_1 c_1$ that fulfils the bounds is given by

$$c_1 = \frac{7.3(s+1)}{s\left((s/25)^2 + (2 \times 0.6/25)s + 1\right)}. \tag{11}$$

On the other hand, let us only use p_2 in the regulation. As long as p_2 is not a minimum phase plant, the QFT method allows two ways of conducting the loop-shaping. The former is depicted in Figure 2(b) where bounds β_{l_2} express the

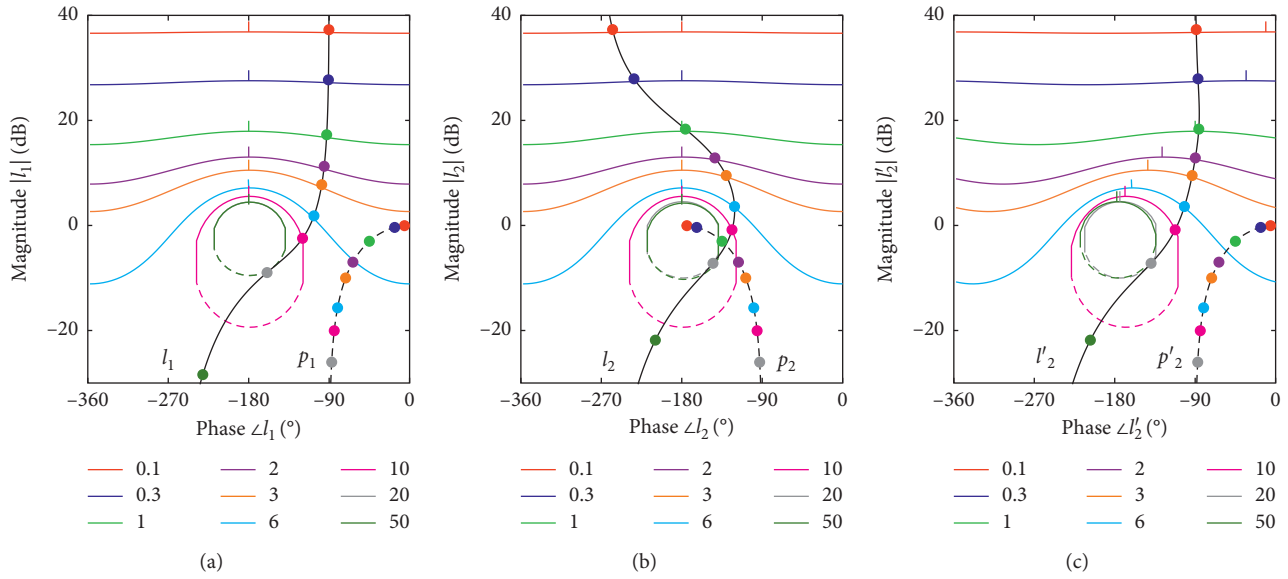

Figure 2: Loop-shaping bounds: (a) β_{l_1}, (b) β_{l_2}, and (c) β'_{l_2}; frequencies in different colours.

feedback demand in terms of $l_t = l_2 = c_2 p_2$, which is not minimum phase and initially ($c_2 = 1$) matches p_2. Another procedure [35, 36] is shown in Figure 2(c). In this case, bounds β'_{l_2} express the feedback demand in terms of l'_2, which initially matches p'_2. This plant corresponds to a p_2 plant whose RHP pole has been mirrored to the LHP (in this example, $p'_2$is equal to p_1). Then, l'_2 and p'_2 are minimum phase, and the phase shift due to p_2 RHP pole has been translated to the bounds β'_{l_2}. Let us note as the relative position between plant frequency responses (p_2 or p'_2) and their respective bounds (β_{l_2} or β'_{l_2}) is the same. As expected, both procedures can yield the same solution, for example,

$$c_2 = \frac{7.3\,(s/0.8 + 1)}{s\left((s/25)^2 + (2 \times 0.7/25)s + 1\right)}. \tag{12}$$

Placing the open-loop function exactly onto the bounds at each design frequency means using the minimum controller gain to achieve the specifications, which favours a smaller control gain beyond the gain cross-over frequency ω_{gc} [32, 37], where feedback becomes useless or even harmful (e.g., high-frequency unmodeled dynamics or sensor noise amplification that can saturate the control input). Then, the minimum quantity of feedback to achieve the specification at each design frequency is the distance between the plant frequency response and the corresponding bound. To quantify it, Rico-Azagra et al. [10] proposed the use of bounds $\beta_c(\omega)$, which were calculated scaling classical bounds $\beta_l(\omega)$ by the nominal plant magnitude$|p_o(j\omega)|$, i.e., $\beta_c(\omega) = (\beta_l(\omega)/|p_o(j\omega)|)$. Performing this on bounds of Figure 2 yields the bounds of Figure 3.

At any frequency, several locations onto the bound are possible for the loop-shaping: one for each phase in the horizontal axis. Thus, the design phase becomes important. Let us analyse the lowest frequency $\omega = 0.1$ in Figure 2. Either the control solution through p_1 (11) or through p_2 (12) contains an integrator to achieve zero steady-state error $r - y$ when a d-step happens. The integrator is usually the first element added during the loop-shaping, which produces a phase lag of −90°. Secondly, the control gain is raised to fulfil the low-frequency bound. After performing these operations in Figures 2(a) and 2(b), the same control element $(7.3/s)$ makes $l_1(j\omega)$ and $l_2(j\omega)$ to fulfil the lowest frequency bounds, $\beta_{l_1}(0.1)$ and $\beta_{l_2}(0.1)$, respectively. Obviously, as long as both plants (7) have the same magnitude at low frequencies, both demand the same control gain. However, the design phase to measure and compare the demanded gain is different: about −90° for l_1 in Figure 2(a) and about −180° for l_2 in Figure 2(b). The exact quantities can be measured on Figures 3(a) and 3(b), respectively. Applying the same reasoning for other frequencies may be a challenging task since it is not so obvious which design phases have to be compared between l_1 and l_2. However, those phases for comparisons become the same on the pictures for l_1 and l'_2, see Figures 2(a) and 2(c). In summary, the bound height (feedback demand) can be easily compared between bounds in Figures 3(a) and 3(c) looking at the same phase. Then, bearing only this criterion in mind, both plants p_1 and p_2 could be indistinctly used to solve the regulation problem since both require the same control gain at any frequency.

However, the fact that two plants require the same feedback when working by their own does not necessarily imply that a collaboration of both would have that quantity of feedback inside an MISO structure. This is only true for minimum-phase plants: for example, the use of two twin plants p_1 would yield two controllers $(c_1/2)$. On the contrary, p_1 and p_2 (or l_1 and l_2) are completely in counter phase at $\omega = 0$, and are only in phase at $\omega = \infty$, as shown in Figures 2(a) and 2(b). Then, they can collaborate over the high frequencies but not over the low frequencies to reduce the individual feedback gain since the function l_t is the vectorial sum of $l_1 + l_2$. Any attempt of designing minimum-phase controllers c_1 and c_2 to make p_1 and p_2 collaborate at low

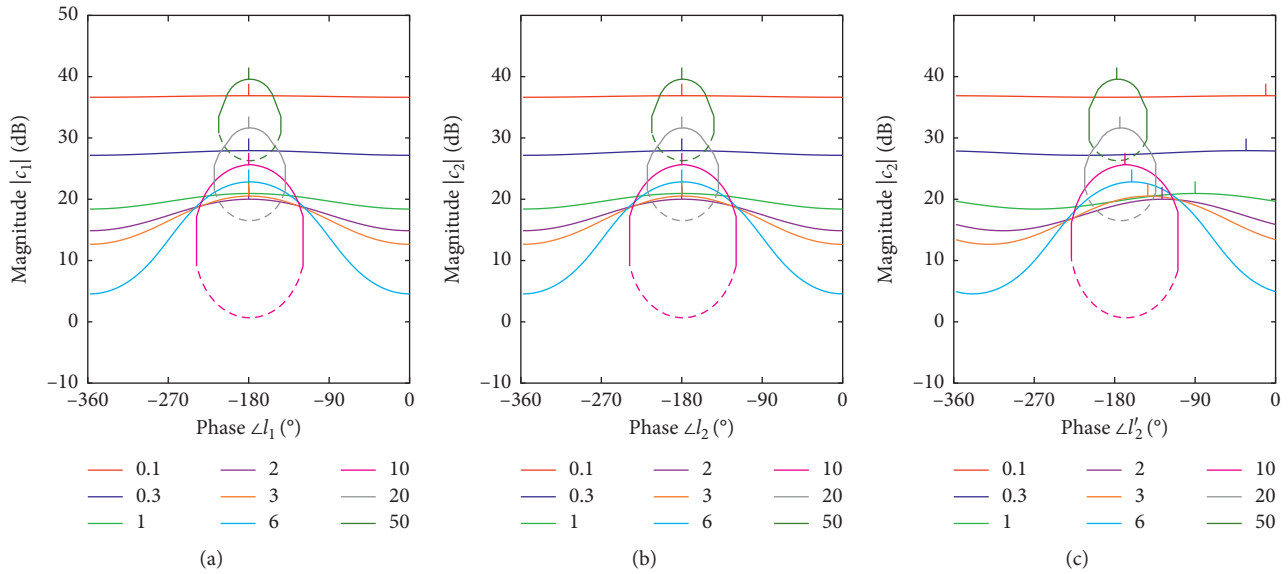

Figure 3: Feedback demand bounds: (a) β_{c_1}, (b) β_{c_2}, and (c) β'_{c_2}; frequencies in different colours.

frequencies would yield controllers of higher gains than c_1 (11) and c_2 (12). As a general rule of thumb, to build a vector $l_t(j\omega)$ with vectors $l_1(j\omega)$ and $l_2(j\omega)$ that have a smaller magnitude than l_t, the phase difference between $l_1(j\omega)$ and $l_2(j\omega)$ has to be less than $\pm 90^\circ$. Looking back at Figure 2, the information about the p_2 phase that can be read in Figure 2(b) has been translated to the bounds that appear shifted in Figure 2(c). Therefore, the phase shift between true plants p_1 and p_2 can be read in the phase shift between bounds β_{c_1} and β'_{c_2} in Figure 3; the vertical segment is taken as a reference that marks the critical phase (-180°) on the bounds.

Once detected at which frequencies the two plants are not out of phase $(\omega \geq 1)$, the amount of feedback that each one would demand becomes of interest. This focuses on the height difference (magnitude in dB) between bounds β_{c_1} and β'_{c_2} in Figure 3 at the design phase Θ_d that is selected for each frequency $\omega \geq 1$. Regardless of the bound height difference, a collaboration would always reduce the gain of controllers (let us remind the loops are not out of phase). However, these reductions may not justify the major complexity of performing the design. A magnitude difference of $20\log 2$ between bounds is a practical guideline to attempt a collaboration, and it is funded on the ideal collaboration of two equal plants, which would reduce the controller gain two times.

Applying previous guidelines, Table 1 summarises the frequency band distribution between the two loops of the example (7). The next step is the loop-shaping of l_1 and l_2 that achieves it, for which viewing the real phase of l_1 and l_2 becomes of great importance. Thus, bounds of the kind of β'_{l_2} in Figure 2(c) are not advisable, but bounds β_{l_2} in Figure 2(b) are preferred. The standard procedure to compute β_{l_i} bounds and to perform iteratively the loop-shaping of each l_i is fully described in [10]. The main steps for the present example are illustrated in Appendix A.

The final elements that integrate the MISO control are

$$c_1 = \frac{63.47s(s/1.3+1)}{(s/0.2+1)(s/0.5+1)\left((s/32)^2+(2\times 0.6/32)s+1\right)}, \tag{13}$$

$$c_2 = \frac{7.01(s/2.7+1)(s/1.7+1)(s/0.23+1)}{s\left((s/0.8)^2+(2\times 0.8/0.8)s+1\right)\left((s/32)^2+(2\times 0.6/32)s+1\right)}. \tag{14}$$

Figure 4 compares different control solutions: c_{1s} is the SISO controller (11), c_{2s} is the SISO controller (12), and $c_1 - c_2$ the MISO control solution (13)–(14). It proves the control gain reduction over the frequencies where the two loops collaborate $(\omega > 1)$. To illustrate the challenges due to RHP dynamics, let us build $p_e = p_1 + p_2$, and design for it a controller

$$c_e = \frac{4(s/0.8+1)(s+1)}{s^2\left((s/35)^2+(2\times 0.7/35)s+1\right)}, \tag{15}$$

to fulfil the specifications. It has forced both plants to collaborate over the whole frequency band, which has implied a huge gain at frequencies where both plants are out of phase $(\omega < 1)$. Over the frequencies where only one branch works, the MISO control is obviously equal to any SISO control $(\omega < 1)$.

Table 1: Frequency band distribution between control inputs of system (7).

ω	0.1	0.3	1	2	3	6	10	20	50
p_1			×	×	×	×	×	×	×
p_2	×	×	×	×	×	×	×	×	×

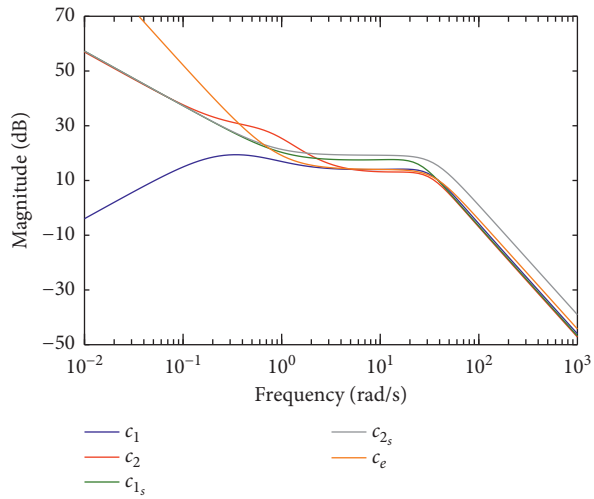

Figure 4: Benchmark of controllers for system (7).

2.3. Proposed Methodology

2.3.1. Stage 1: Feedback Sharing at Each Frequency of Design. This first stage distributes the control bandwidth among the plants that could contribute to the robust regulation problem (2)–(3) in order to reduce as much as possible the amount of feedback (gain) that is demanded by the controllers at each frequency. These decisions are made by the comparison of control bounds $\beta'_{c_i}(\omega)$, $i = 1, \ldots, n$.

$\beta'_{c_i}(\omega)$ quantifies the necessary feedback $|c_i(j\omega)|$ at each discrete frequency ω in the event that a single plant $p_i(j\omega)$ worked to achieve the robust control requirements. In order to calculate the said bounds, nominal MP plants p'_{o_i} must be employed. For those plants that were not minimum phase, p'_{o_i} is obtained from p_{o_i} by mirroring all RHP dynamics into the LHP and neglecting any possible delay (it fulfils $|p_{o_i}(j\omega)| = |p'_{o_i}(j\omega)|$). Nominal plants can be any $\mathbf{P}(j\omega)$ of the uncertainty set (1). Then, common QFT bounds on the nominal open-loop function $l'_{o_i}(j\omega)$ are computed, which yields $\beta'_{l_i}(\omega)$. These are computed in the event that only $p_i(j\omega)$ assumes the regulation task. Eventually, $\beta'_{c_i}(\omega) = (\beta'_{l_i}(\omega)/|p'_{o_i}(j\omega)|)$. Bounds $\beta'_{c_i}(\omega)$shift with respect to−180°an amount equal to the phase difference between $p_{o_i}(j\omega)$ and $p'_{o_i}(j\omega)$.

The $\beta'_{c_i}(\omega)$ bound comparison among loops $i = 1, \ldots, n$ focuses at the desired design phase $\Theta_d \in (-360°, 0°]$, which is particularly chosen for each frequency and is unique for all loops (Θ_d is the phase in which the nominal open loop l_{o_i} will be modified through the addition of gain, pole, or zero elements during the loop-shaping at Stage 2). The criteria for the control bandwidth distribution are

(a) *Criterion* 1: m plants ($m \geq 2$) can collaborate at ω, if the phase differences between the m bounds $\beta'_{c_{k=1,\ldots,m}}$ are less than $\pm 90°$ and if the heights of the said bounds do not differ from each other more than $\pm 20 \log m$ dB at the design phase Θ_d. Additionally, there is no bound $j \neq k$ of lesser height. Consequently, the remaining plants $j \neq k$ should be inhibited, reducing their control gain as much as possible at ω during the design stage.

(b) A single plant is in charge of the regulation at ω if criterion 1 is not met.

(c) The highest m is sought ($m \leq n$) since the gain saving on each one of the m branch controllers is proportional to m, i.e., to the number of plants that collaborate.

The amount $20 \log m$ is a practical guideline. It is funded on the ideal collaboration of m equal plants, which would reduce the controller gain m times. The phase shifting between bounds is vital when plants contain RHP dynamics and delays. This argument condition determines if the loops are not out of phase, and therefore, $|l_{o_t}(j\omega)| \approx |\sum l_{o_k}(j\omega)|$ can be built with $|l_{o_k}(j\omega)| \leq |l_{o_t}(j\omega)|$.

2.3.2. Stage 2: Design of Controllers. The designs of the $i = 1, \ldots, n$ loops are carried out sequentially such that $l_{o_i}(j\omega)$ fulfils the specifications (bounds $\beta_{l_i}(\omega)$) according to the feedback sharing that was established in Stage 1. The general procedure was provided in [10], and it does not depend on the plants being MP or not. Bounds β_{l_i} are computed and referenced to the true plant p_{o_i} being MP or not.

3. Application: MISO Control of a Continuous Stirred-Tank Reactor

In this section, the benefits of the proposed methodology are shown on a recurrent benchmark of the chemical and materials industry, the continuous stirred-tank reactor (CSTR) of unquestionable importance in the transformation of raw materials into valuable chemicals or products [6, 38, 39].

3.1. The Process and the Control Design. The control setup of the MISO plant is depicted in Figure 5. A coolant flow (usually water) through a jacket $u_2 = F_j$ removes the necessary energy to prevent the exothermic and irreversible reaction runaway and to regulate the reactor temperature $y = T_r$. Due to the limited heat-removal capacity of the coolant flow, the manipulation of the reactant flow $u_1 = F$ can contribute to the temperature control. The linear dynamic models linked to these manipulated inputs are p_1 and p_2. The work [6] presented a MISO control strategy inside a series control architecture following the VPC of [40]. In this paper, the parallel architecture of Figure 1 is used. The jacket coolant flow (the fastest actuation) midranges around $r_{u_2} = r_{F_j}$, while large reaction temperature excursions are compensated with the feed flow rate (the slowest actuation). Thus, beyond the dual-input collaboration in disturbance

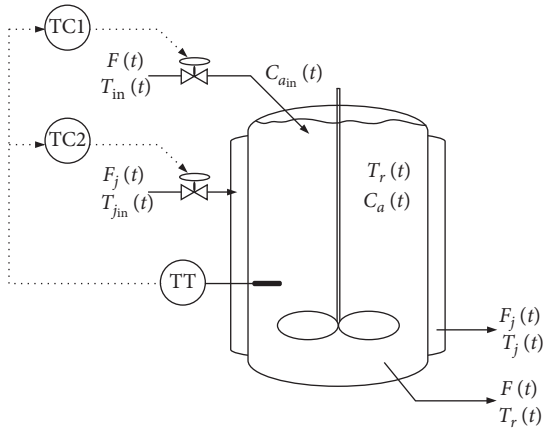

Figure 5: MISO control of CSTR.

compensation, the MISO strategy can achieve the highest possible production rate: F is maximised when F_j set point is set to maximum. Three disturbance inputs are being considered: the feed concentration $d_1 = C_{a_{\text{in}}}$, the feed temperature $d_2 = T_{\text{in}}$, and the inlet coolant temperature $d_3 = T_{j_{\text{in}}}$, whose contributions to the output T_r deviation are being represented by linear plants p_{d_1}, p_{d_2}, and p_{d_3}, respectively. Appendix B details the procedure on how to obtain all linear plant models from nonlinear differential equations of dynamic mass and energy balances [6]. Small-signal linearisation is executed about the system operating point

$$\mathbf{q}_j = \left[T_{r_e}, F_e, F_{j_e}, C_{a_{\text{in}_e}}, T_{\text{in}_e}, T_{j_{\text{in}_e}}\right], \tag{16}$$

which relates the equilibrium (subscript "e") of main process variables. A discrete set of 192 possible operating points is being considered (see Appendix B), which yields uncertainty about linear plant models. Thus, there is a plant matrix $\mathcal{P}$ (1) that collects 192 vectors $\mathbf{P}(\mathbf{s}; \mathbf{q_j}) = [p_1, p_2, p_{d_1}, p_{d_2}, p_{d_3}]$. Figure 6 shades the envelopes of magnitude frequency responses of all plant cases and highlights the nominal plants

$$p_{1_o} = \frac{31.1342\,(-s/0.002224 + 1)\,(s/0.003147 + 1)}{(s/0.003329 + 1)\left((s/0.00032696)^2 + (2 \times 0.6697/0.00032696)s + 1\right)}, \tag{17}$$

$$p_{2_o} = \frac{-8.7745\,(s/0.0008615 + 1)}{(s/0.003329 + 1)\left((s/0.00032696)^2 + (2 \times 0.6697/0.00032696)s + 1\right)}, \tag{18}$$

$$p_{d_{1_o}} = \frac{3.0482\,(s/0.003147 + 1)}{(s/0.003329 + 1)\left((s/0.00032696)^2 + (2 \times 0.6697/0.00032696)s + 1\right)}, \tag{19}$$

$$p_{d_{2_o}} = \frac{1.6408\,(s/0.003147 + 1)\,(s/0.0008615 + 1)}{(s/0.003329 + 1)\left((s/0.00032696)^2 + (2 \times 0.6697/0.00032696)s + 1\right)}, \tag{20}$$

$$p_{d_{3_o}} = \frac{4.5446\,(s/0.0008615 + 1)}{(s/0.003329 + 1)\left((s/0.00032696)^2 + (2 \times 0.6697/0.00032696)s + 1\right)}, \tag{21}$$

which correspond to the nominal values of equilibrium (16): $T_{r_o} = 350\,\text{K}$, $F_o = 4.377 \times 10^{-3}\,(\text{m}^3/\text{s})$, $F_{j_o} = 11.3 \times 10^{-3}\,(\text{m}^3/\text{s})$, $C_{a_{\text{in}_o}} = 8.01\,(\text{kmol}/\text{m}^3)$, and $T_{\text{in}_o} = T_{j_{\text{in}_o}} = 294\,\text{K}$.

Regarding Figure 6, the gain of p_1 is higher than that of p_2 over the whole frequency band; this reveals the feed flow F is the most powerful regulation variable. Its counterpart is the feed temperature T_{in} which gets a significant impact on dynamic controllability. When the feed is colder than the reactor ($T_{\text{in}} < T_r$), the immediate effect of increasing the feed flow rate is a temporary decrease in the reactor temperature, i.e., p_1 behaves as a nonminimum phase (NMP) plant. In particular, the RHP-plane uncertain zero of p_1 at $\omega \in [0.0014, 0.0029]$ makes the p_1 participation unsuitable in control tasks over high frequencies. Then, a convenient frequency distribution of MISO dynamic controllability is of importance and can be quantitatively accomplished through the robust frequency domain method that this paper develops. Let us also mention that p_2 plant has a negative gain since raising the jacket flow rate F_j makes the reactor temperature T_r to drop.

Three performance specifications for robust disturbance rejection are defined following (2), being p_d equal to p_{d_1}, p_{d_2}, and p_{d_3}, respectively. The required performance is that in the case of a maximum disturbance happens, the reactor temperature deviation has to be less than 1 K; and this maximum deviation has to be reduced to 0.25 K no later than 2.5 h after and fully extinguished in the steady state (settling time less than 4.0 h to stay within a $\pm 5\%$ band). To ensure these conditions, the performance upper model is

$$W_d(j\omega) = \frac{6796\,j\omega}{(j\omega/0.0004 + 1)^2}. \tag{22}$$

Besides, two robust stability specifications (3) adopt as upper tolerance

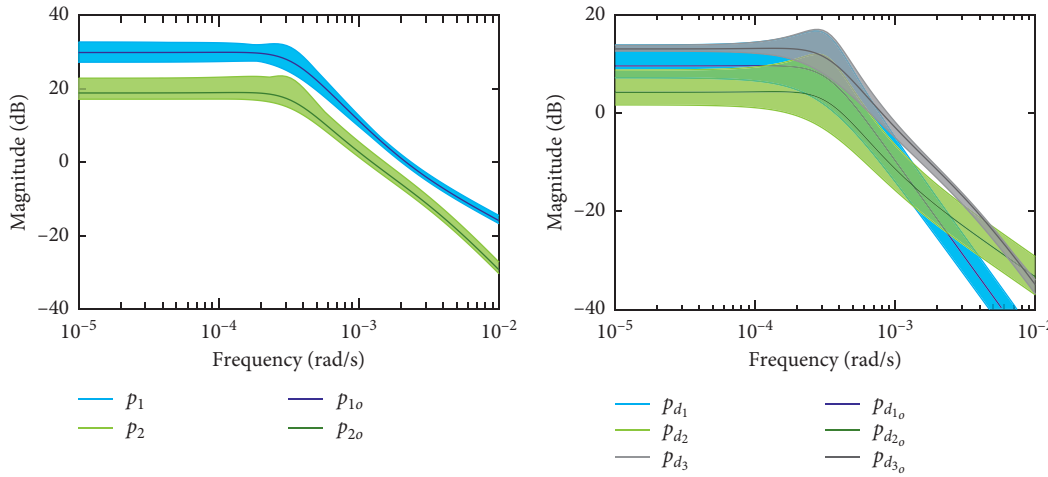

Figure 6: CSTR. Frequency responses of scaled plants.

$$W_{s_{i=1,2}} = 1.462, \tag{23}$$

to guarantee minimum phase margins of 40° on each of the two loops (4). The discrete set of ω-frequencies to compute QFT bounds is

$$\Omega = [1, 2, 3, 5, 8, 10, 50] \times 10^{-4}\ [\text{rad/s}]. \tag{24}$$

3.1.1. Stage 1: Feedback Sharing at Each Frequency of Design. Bounds β_{c_i}' are calculated. Figure 7 depicts them at the most illustrative frequencies, which yields the following conclusions according to the criteria in Section 2.3:

At low frequencies $\omega \le 3 \times 10^{-4}$, bounds $\beta_{c_1}'(\omega)$ and $\beta_{c_2}'(\omega)$ are found phase-shifted less than $\pm 90°$. However, $\beta_{c_1}'(\omega)$ are located over $20 \log 2 = 6$ dB lower than $\beta_{c_2}'(\omega)$, which make the participation of $p_2(j\omega)$ useless in the regulation. Thus, the branch of $p_1(j\omega)$ should assume only the y regulation, and the branch of $p_2(j\omega)$ should be switched off at $\omega \le 3 \times 10^{-4}$.

At medium frequencies $3 \times 10^{-4} < \omega \le 8 \times 10^{-4}$, bounds $\beta_{c_1}'(\omega)$ and $\beta_{c_2}'(\omega)$ are found phase-shifted less than $\pm 90°$ and present a similar height around $\Theta_d = -90°$. Thus, plants $p_1(j\omega)$ and $p_2(j\omega)$ can collaborate over this interval of frequencies.

At frequencies $\omega > 8 \times 10^{-4}$, the phase shifting between bounds $\beta_{c_1}'(\omega)$ and $\beta_{c_2}'(\omega)$ increases beyond $\pm 90°$ such that the collaboration between plants is no longer possible. Thus, $p_2(j\omega)$ should assume the control tasks while $p_1(j\omega)$ should be inhibited by making $l_1(j\omega) \approx 0$, which avoids the limitations introduced by the RHP zero of p_1.

3.1.2. Stage 2: Loop-Shaping of Controllers. To fulfil the objectives set in Stage 1, the loop-shaping of the two nominal open-loop functions is carried out following a sequential methodology as detailed in [10]. Figure 8 shows the final arrangement of bounds $\beta_{l_{i=1,2}}(\omega)$ at design frequencies (24) and the nominal open-loop transfer functions $l_{o_{i=1,2}}(j\omega)$ that satisfy them. Let us note that l_{o_1} contains an RHP zero. The resulting controllers are

$$c_1 = \frac{3.2 \times 10^{-5}\,(s/0.0003 + 1)\,(s/0.0084 + 1)}{s\,(s/0.0017 + 1)^2\left((s/0.015)^2 + (2 \times 0.5/0.015)s + 1\right)}, \tag{25}$$

$$c_2 = \frac{-0.37\,(s/0.0003 + 1)\,(s/00018 + 1)}{(s/0.001 + 1)\left((s/0.0024)^2 + (2 \times 0.8/0.0024)s + 1\right)}. \tag{26}$$

3.2. Results: Analysis and Comparatives. Figure 9 proves the fulfilment of control specifications for the whole set of 192 plant cases: Figure 9(a) shows what concerns the robust rejection at the output of the three disturbances and the performance specification (2) and (22), and Figure 9(b) shows what concerns the robust stability of the two loops and the stability specification (3) and (23). Figure 10 illustrates the frequency band allocation between both loops: $l_t(j\omega)$ matches $l_1(j\omega)$ over low frequencies, $l_t(j\omega)$ matches $l_2(j\omega)$ over high frequencies, and $l_t(j\omega)$ matches $l_1(j\omega) + l_2(j\omega)$ over midfrequencies.

Closed-loop time responses of main system variables are shown in Figure 11. These results have been obtained using the proposed control system in the nonlinear model of CSTR (at this point it is recommended to see Appendix B for a full understanding of the physical units and experiments). The simulation shows the system behaviour for step-type disturbances in the feed temperature ($\delta T_{\text{in}} = 5$ K at $t = 2$ h), in the coolant temperature ($\delta T_{j_{\text{in}}} = -5$ K K at $t = 8$ h), and in the feed concentration ($\delta C_{a_{\text{in}}} = 5\% C_{a_{\text{in}_o}}$ at $t = 14$ h). Measured output T_r incorporates sensor noise, which is generated by a band-limited white noise source $v(t)$ (noise power: 0.02; sample time = 100). Several set points on the coolant flow rate r_{F_j} between 65% and 85% of F_j maximum capacity have been tested. In all cases, the reactor temperature T_r deviates less than the maximum permitted (1 K) and recovers the set point (350 K) in less than 4.0 h after any

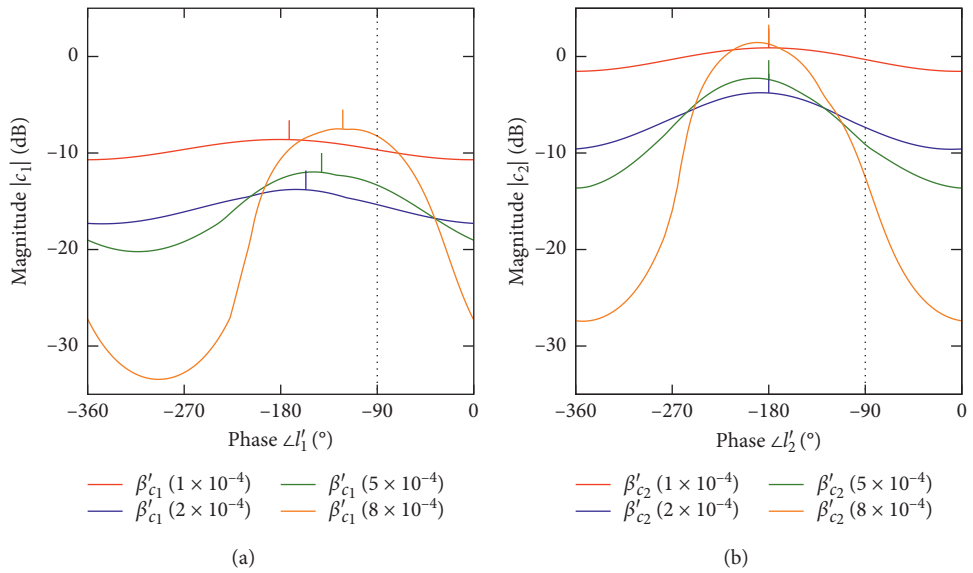

Figure 7: CSTR. Feedback demands in the event of single plant intervention.

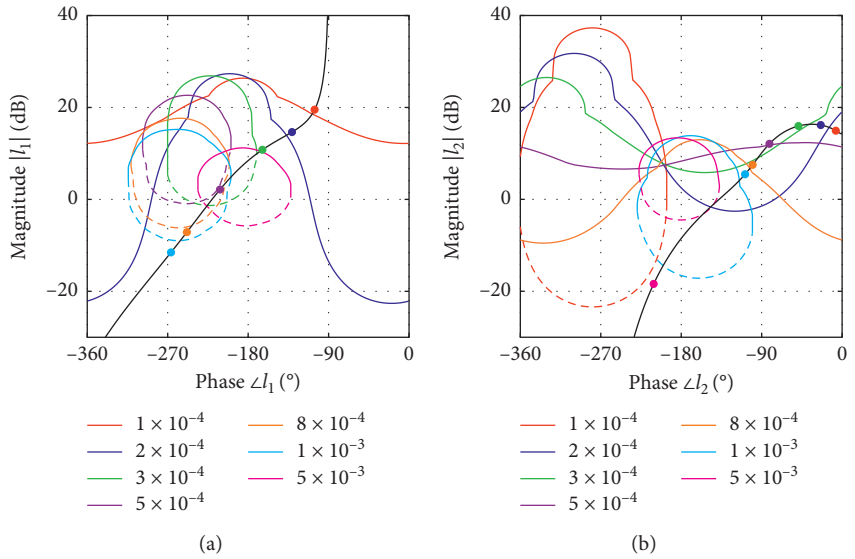

Figure 8: CSTR. Loop-shaping of controllers.

disturbance happens. The steady-state feed flow F increases when the coolant set point r_{F_j} increases. This proves the smart VPC strategy [6] of indirectly maximizing the production rate by using a dual-input control. The collaboration of inputs (plants) in disturbance rejection is as follows: when a disturbance happens, the coolant flow rate F_j quickly reacts to compensate the reactor temperature deviation. Then, as the feed flow F takes control of the situation, F_j is progressively reset. Eventually, F_j returns to r_{F_j} after approximately 30 min. F cannot return to a particular set point r_F while any disturbance persists. However, r_{F_j} can be wisely moved to bring F towards a particular range: a larger r_{F_j} involves a larger F, which increases the production rate; on the other hand, a smaller r_{F_j} pursues saving the amount of F_j. Both F and F_j move between their margins of operation [0% and 100%], despite the fact perturbations are of maximum amplitude. The evolution of other internal system variables, like T_j and C_a, is also included in the simulations.

Following, there are argued benefits of MISO control versus SISO control. In this last case, the same robust control

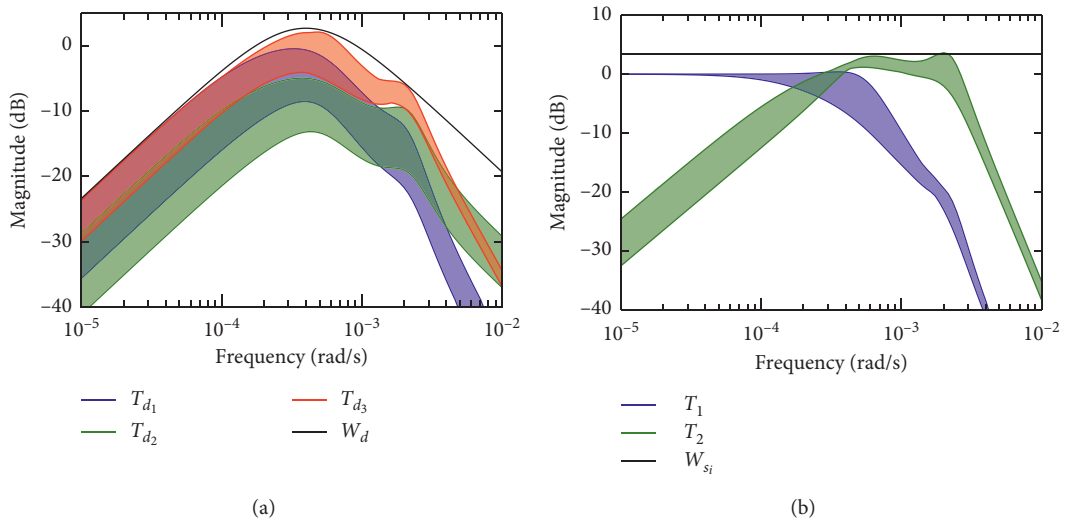

Figure 9: MISO control of CSTR. Closed-loop frequency responses.

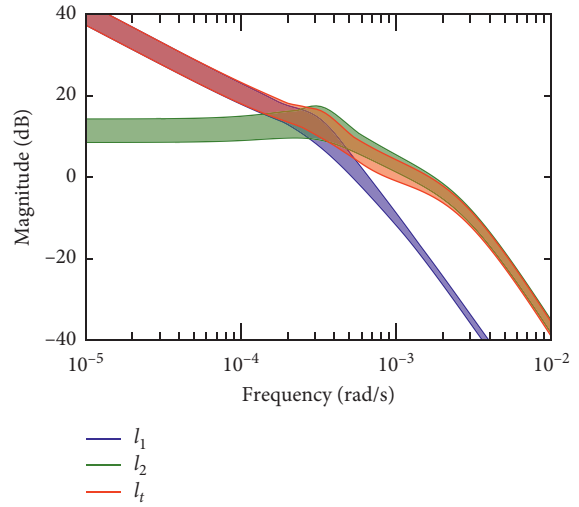

Figure 10: MISO control of CSTR. Open-loop frequency responses.

specifications are being satisfied with solely a loop intervention. Let us denote F-SISO control when $u_1 = F$ is in charge of the regulation tasks, and thus $u_2 = F_j$ remains at a constant value. In that case, the control design process yields

$$c_{1_{\text{SISO}}}(s) = \frac{3.1354 \times 10^{-5}(s/0.0012 + 1)(s/0.0004 + 1)(s/0.00045 + 1)}{s(s/0.003 + 1)(s/0.006 + 1)}. \tag{27}$$

On the other hard, let us denote F_j-SISO control when $u_2 = F_j$ is in charge of the regulation task and $u_1 = F$ remains at a constant value. Thus, the single controller results

$$c_{2_{\text{SISO}}}(s) = \frac{-1.2402 \times 10^{-4}\left(\left(s/\left(3.488 \times 10^{-4}\right)\right)^2 + \left(2 \times 0.76/\left(3.488 \times 10^{-4}\right)\right)s + 1\right)}{s(s/0.001 + 1)(s/0.004 + 1)}. \tag{28}$$

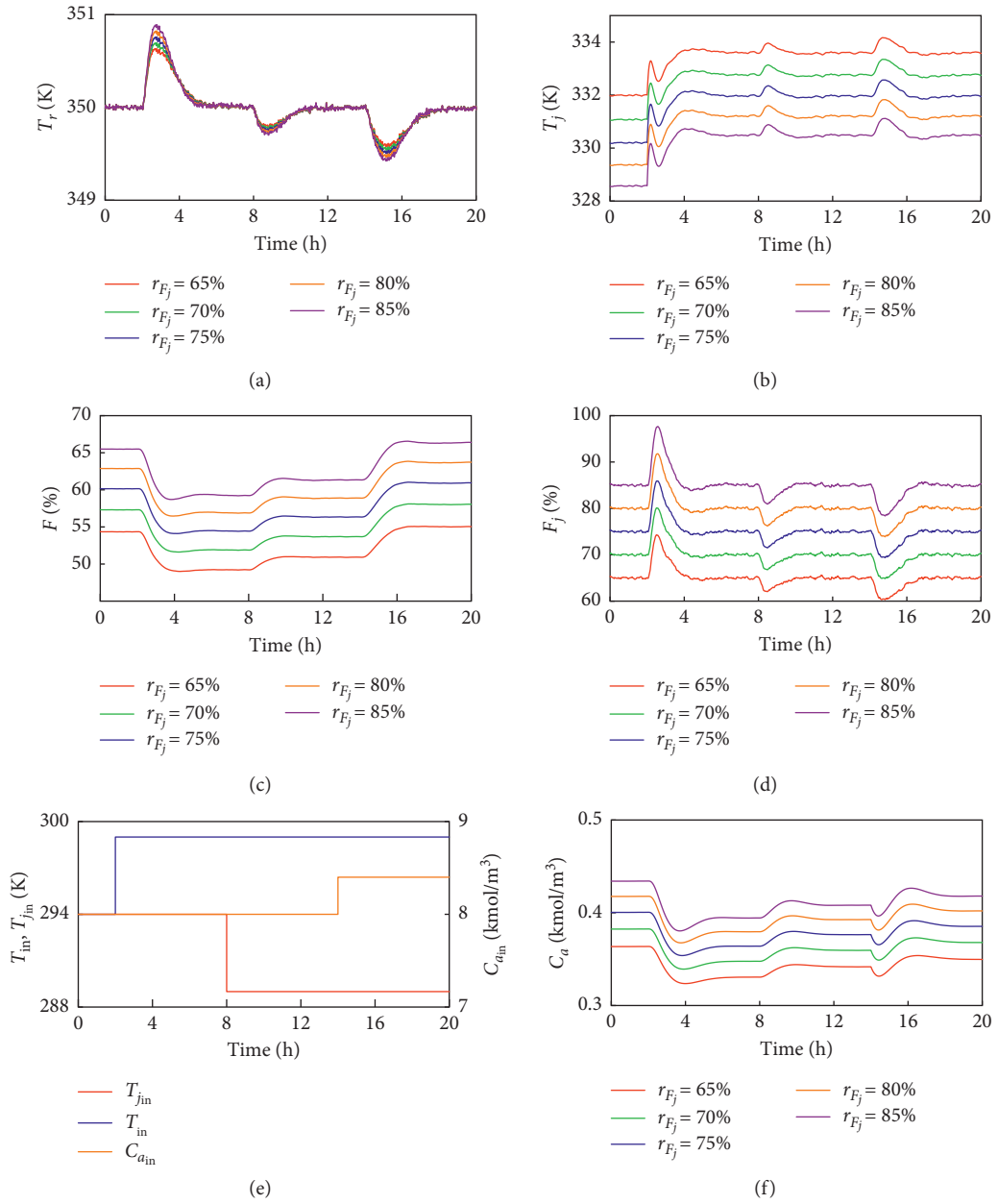

Figure 11: MISO control of CSTR. Closed-loop time responses.

Figures 12 and 13 depict frequency and time responses, respectively; their first and second columns of plots correspond to F-SISO and F_j-SISO control, respectively. The beam of frequency responses in Figures 12(c)–12(f) corresponds to the 192 cases of plant uncertainty. The time experiments of Figure 13 are run in a nonlinear simulator of CSTR and under the same conditions than the MISO control. In particular, Figure 11(e) details the changes of disturbance inputs, and five cases are being considered: for F-SISO, the coolant flow $F_j(t)$ takes constant values {65%, 70%, 75%, 80%, and 85%}, and for F_j-SISO, the feed flow $F(t)$ adopts constant values {55%, 57.5%, 60%, 62.5%, and 65%}. Correlation between time and frequency responses agrees with the superiority of MISO over SISO control as follows.

The required performance and stablility cannot be achieved by p_1 on its own due to the limited bandwidth imposed by the RHP zero; F-SISO (27) yields a reasonable trade-off solution between disturbance rejection and stability commitments. Figure 12(e) shows how T_{d_1} and T_{d_3} slightly violate W_d over midfrequencies, despite the fact this worsening is hardly noticeable in Figure 13(a) in comparison with Figure 11(a). Additionally, Figure 12(e) shows violations of robust stability W_s, which means a reduction of the phase margin from 40° to 35°. Nevertheless, the major drawback of F-SISO control can be noticed from the

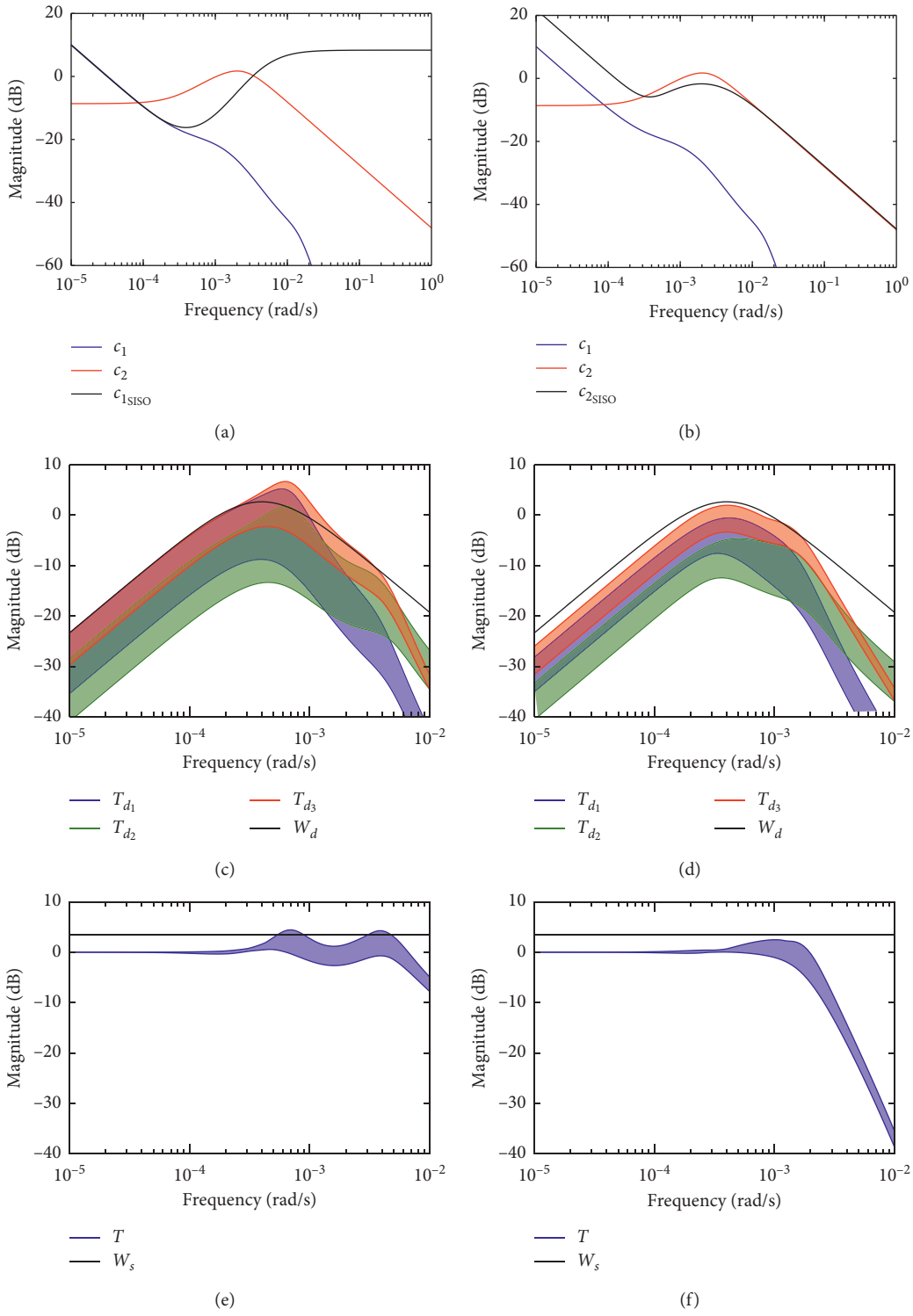

Figure 12: SISO control of CSTR. Frequency responses: (a), (c), and (e) F-SISO; (b), (d), and (f) F_j-SISO.

comparison of control gains in Figure 12(a). p_1-plant, which has an RHP zero at $\omega \in [0.0014, 0.0029]$, has been forced to work beyond $\omega = 0.0008$ at the expense of a huge increase of the controller gain $|c_{1_{SISO}}(j\omega)|$ over high frequencies. It produces an inadmissible sensor noise amplification at the control input $F(t)$,see Figure 13(c), which did not happen in MISO control—see Figures 11(c) and 11(d). In that case, a minimum phase p_2-plant worked over the high-frequency band, despite apparently being less powerful (less gain) than a nonminimum phase p_1-plant, see Figure 6(a). Therefore, $|c_2(j\omega)| \ll |c_{1_{SISO}}(j\omega)|$ over high frequencies reports important benefits. Additionally, $|c_1(j\omega)| \approx |c_{1_{SISO}}(j\omega)|$ at low

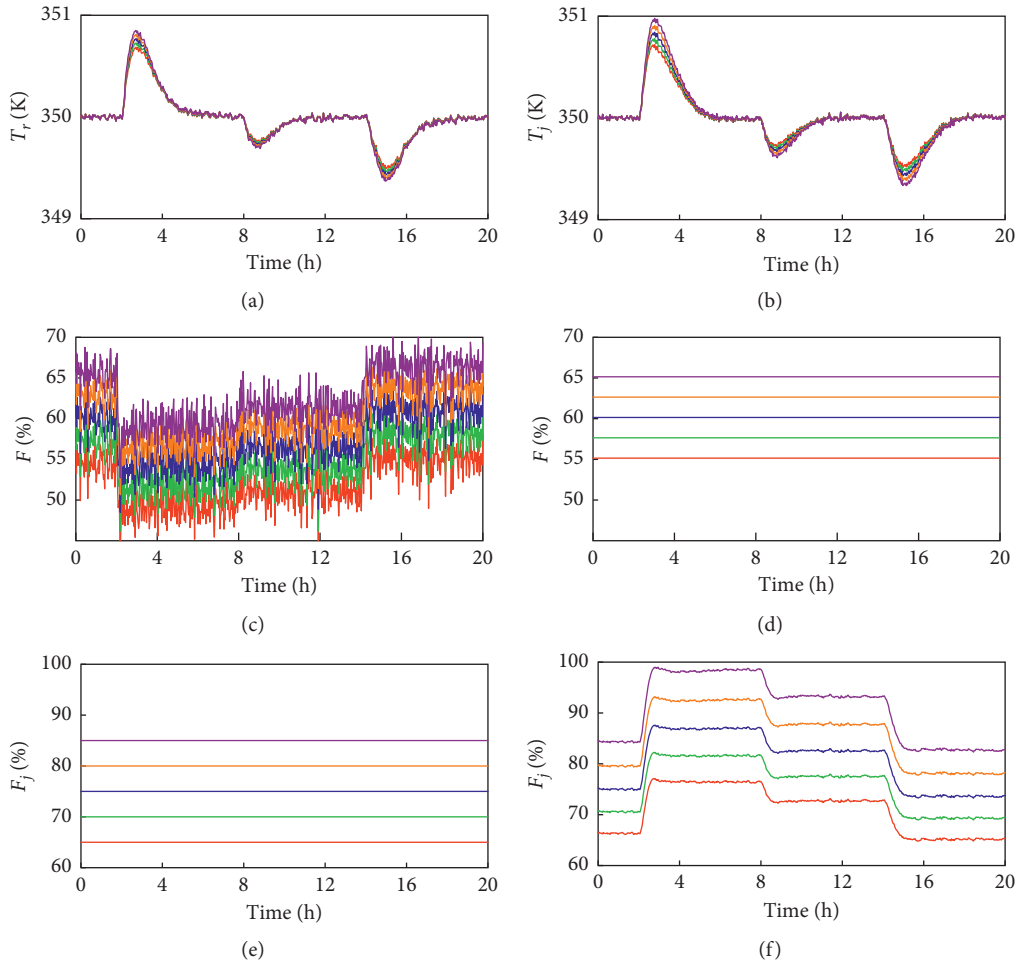

Figure 13: SISO control of CSTR. Closed-loop time responses: (a), (c), and (e) F-SISO; (b), (d), and (f) F_j-SISO.

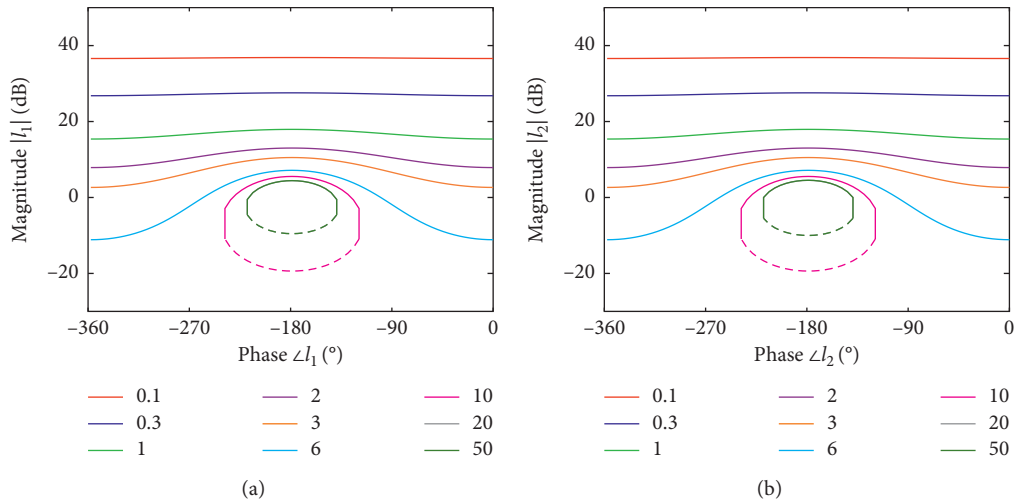

Figure 14: Continued.

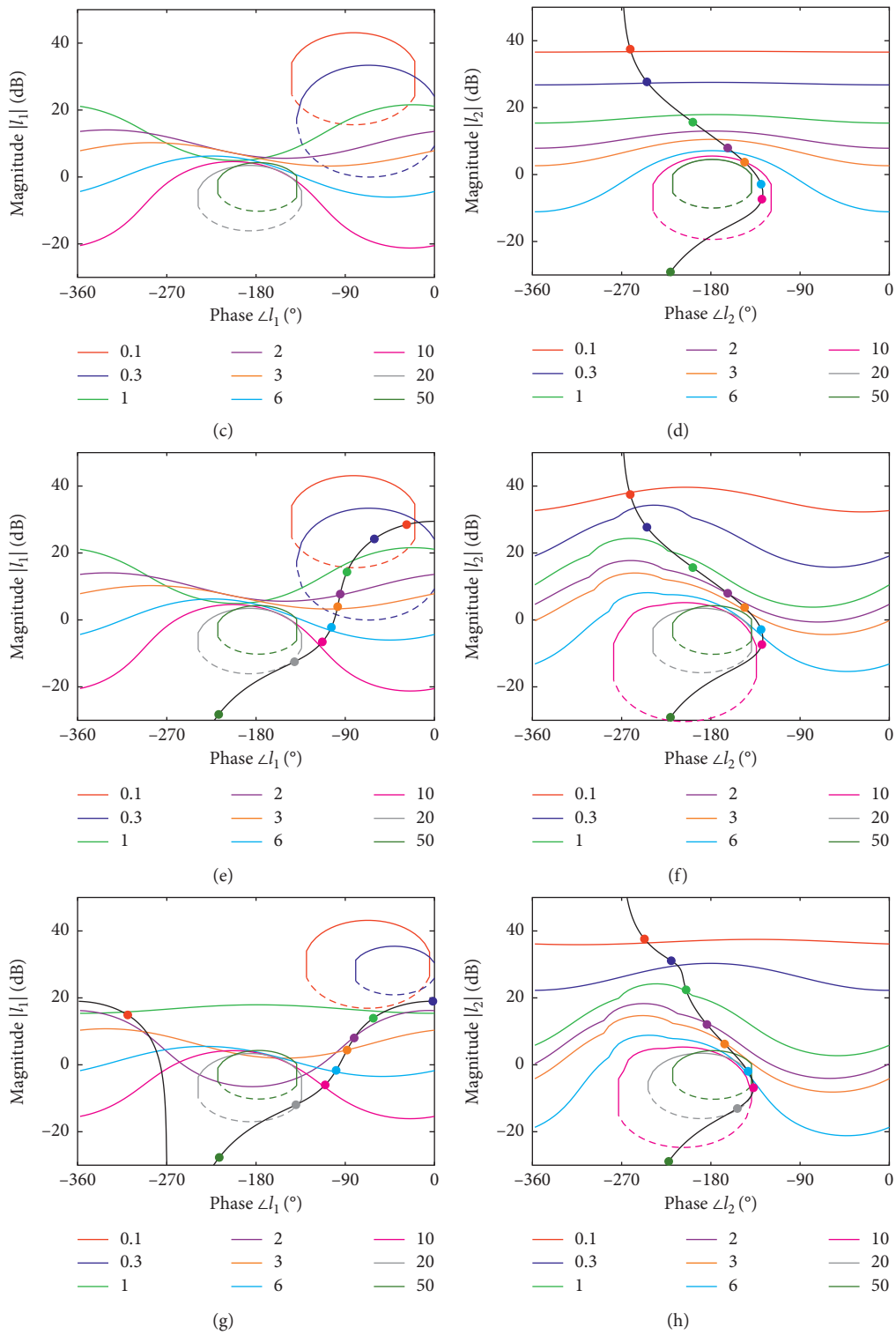

FIGURE 14: Loop-shapings with Table 1 aims: (a) loop-shaping l_1^0, (b) loop-shaping l_2^0, (c) loop-shaping l_1^{I}, (d) loop-shaping l_2^{I}, (e) loop-shaping l_1^{II}, (f) loop-shaping l_2^{II}, (g) loop-shaping l_1^{III}, and (h) loop-shaping l_2^{III}.

frequencies, which means that the same $F(t)$ is needed to manage the steady states at Figure 13(c) and at Figure 11(c) if the noise components are dismissed from Figure 13(c).

On the contrary, Figures 12(d) and 12(f) check how the minimum phase p_2-plant can achieve the specifications on its own, which means the temperature recovery $T_r(t)$ meets

the time requirements in Figure 13(b) as it happened in Figure 11(a). The counterpart is that the p_2-plant has to do the p_1-plant work at $\omega \leq 0.0003$, despite the fact p_2 is less powerful (gain) than p_1, see Figure 6(a). It results in higher control gains $|c_{2_{\text{SISO}}}(j\omega) \gg |c_1(j\omega)|$ over low frequencies and specifically at $\omega = 0$. In this way, δF_j in each steady state, see Figure 13(f), is larger than δF in each steady state, see Figure 11(c). As an example, after the step change of the feed temperature ($\delta T_{\text{in}} = 5$ K) at $t = 2$ h, the SISO control (case $F = 65\%$) requires a steady-state variation δF_j of 14%, which approaches the available maximum of F_j; meanwhile, the MISO control (case $r_{F_j} = 85\%$) only required a steady-state variation δF of 5%. Additionally, $|c_2(j\omega)| \approx |c_{2_{\text{SISO}}}(j\omega)|$ at high frequencies, which means the same sensor noise amplification at F_j in Figure 13(f) and in Figure 11(d).

In summary, the superiority of MISO versus the SISO control of CSTR relies on the following facts. A better performance for reactor temperature control can be achieved without high sensor noise amplification at the manipulated inputs, which prevents actuator saturation and fatigue. One input F is in charge of the steady state, which resets the fastest input F_j to prescribed values r_{F_j}. This is important from two points of view. As the fastest input returns to the set point after a disturbance rejection, it preserves the initial manoeuvring range to quickly react to new disturbances. Additionally, r_{F_j} gives places to infinite combinations of manipulated inputs to achieve the same reactor temperature. Some convenient ones are increasing r_{F_j} to maximize the production rate F or decreasing r_{F_j} to reduce the coolant cost F_j.

4. Conclusions

This work has presented a control solution where multiple inputs to a system can be used to govern its single measurable output. The method aimed a set of parallel controllers with the smallest possible gain at each frequency to achieve prescribed robust stability and robust performance in disturbance rejection. At a frequency, the gain of a branch controller was reduced when the magnitude of the associated plant contributed significantly to increasing the total magnitude of the vector sum of the branches (each branch included a controller and a plant). However, this was not easily to foresee due to counter-phase effects of RHP dynamics (or delays), due to uncertainties in the plant models, or due to the intervention of a great number of plants (inputs). The quantitative feedback theory (QFT) framework succeeds in the challenge. Then, some QFT control bounds were proposed to quantify the capacity of each plant to achieve the performance at each frequency. The lower the height the control bounds represented, the lower the control magnitude required by the associated plant. Besides, RHP dynamics and delays resulted in a phase shifting of these control bounds. Thus, comparing not only their relative magnitude but also their relative phase, the criteria of plant collaboration or inhibition at certain frequency to yield the control solution of the smallest gain were established. At the end of this first stage, the frequency band was allocated amongst the plants. At a second stage, the loop-shaping of the controllers carried out the predefined regulation sharing. Classical QFT bounds were computed to guide each loop-shaping. To illustrate the method, the MISO control of an unstable system was conducted.

As a challenging example, the temperature of a continuous stirred-tank reactor was regulated through the coolant and feed flows pulling together along frequency bands that slightly overlapped. The feed flow capacity dominated the steady state, but from a dynamic point of view, it involved a temporary decrease in the reactor temperature. This nonminimum phase behaviour made useful the contribution of the coolant flow in the high-frequency band to improve the performance. Several feed flow temperatures, cooling flow temperatures, and reactant concentrations were considered. The provided control design method achieved a quantitative frequency distribution of MISO dynamic controllability in order to meet the prescribed robust performance and stability. Besides, a conveniently chosen set point for the coolant flow (midrange variable) governed indirectly the feed flow in the steady state, which conditioned the production rate.

Appendix

A. Design of Controllers for a Dual-Input System with an Unstable Plant

As part of the example in Section 2.2, the sequential loop-shaping of c_1 and c_2 is performed with Table 1 aims. Figure 14 illustrates the procedure in detailed steps (marked with superscripts). Steps 0, I, and II belong to the same first iteration, which explains the design of c_1 and c_2. Further iterations (step III) are required to optimize both designs looking for the strictly minimum amount of feedback (gain) at each frequency, which usually trades off with a reasonable order of the controllers.

0 Initial bound computation is drawn with $c_1^0 = 0$ for the loop 1 (Figure 14(a)) and with $c_2^0 = 0$ for the loop 2 (Figure 14(b)).

(I) Loop-shaping of l_2 (see Figure 14(d)): to achieve $l_t \approx l_2$ at $\omega < 1.0$, l_2 is located onto bounds $\beta_{l_2}(0.1)$ and $\beta_{l_2}(0.3)$. At $\omega \geq 1$, l_2 will collaborate with l_1, so l_2 can slightly violate the bounds. After step I, the controllers are

$$c_1^{\text{I}} = c_1^0 = 0,$$
$$c_2^{\text{I}} = \frac{7.5(s/1.8 + 1)}{s\left((s/32)^2 + (2 \times 0.6/32)s + 1\right)}. \tag{A.1}$$

As a consequence, new bounds β_{l_1} result in Figure 14(c).

(II) Loop-shaping of l_1 (see Figure 14(e)): l_1 should fulfil all the bounds if no more iterations were desired. However, this would make hard the design, and require a high-order controller. Further iterations are recommended. A simpler controller is designed despite the fact it temporarily violates the bounds that are hard to satisfy ($\omega = 1$). It yields

Table 2: CSTR: parameters and nominal equilibrium values.

Volume of the vessel V_r	m^3	101.6
Reaction rate pre-exponential factor k_0	s^{-1}	20.75×10^6
Activation energy E	$J\,kmol^{-1}$	69.71×10^6
Universal gas constant R	$J\,kmol^{-1}\,K^{-1}$	8.314×10^3
Heat of reaction λ	$J\,kmol^{-1}$	-69.71×10^6
Process density ρ	$kg\,m^{-3}$	801
Process heat capacity c_p	$J\,kg^{-1}\,K^{-1}$	3137
Coolant density ρ_j	$kg\,m^{-3}$	1000
Coolant heat capacity c_{p_j}	$J\,kg^{-1}\,K^{-1}$	4183
Overall heat transfer coefficient U	$W\,m^{-2}\,K^{-1}$	851
Jacket heat transfer area A_j	m^2	101.25
Jacket volume V_j	m^3	10.12
Nominal feed concentration $C_{a_{\text{in}_o}}$	$kmol\,m^{-3}$	8.01
Nominal feed temperature T_{in_o}	K	294.00
Nominal inlet coolant temperature $T_{j_{\text{in}_o}}$	K	294.00
Nominal reactant concentration C_{a_o}	$kmol\,m^{-3}$	0.4
Nominal reactor temperature T_{r_o}	K	350.00
Nominal jacket temperature T_{j_o}	K	330.20
Nominal feed flow rate F_o	$m^3\,s^{-1}$	4.40×10^{-3}
Maximum feed flow rate $F_{\max}$	$m^3\,s^{-1}$	7.30×10^{-3}
Nominal jacket flow rate F_{j_o}	$m^3\,s^{-1}$	11.3×10^{-3}
Maximum jacket flow rate $F_{j_{\max}}$	$m^3\,s^{-1}$	15×10^{-3}

$$c_1^{\text{II}} = \frac{29.74\,(s/1.3+1)}{(s/0.2+1)\left((s/32)^2+(2\times 0.6/32)s+1\right)},$$
$$c_2^{\text{II}} = c_2^{\text{I}}. \tag{A.2}$$

New bounds β_{l_2} result in Figure 14(f).

(III) Both loops are iteratively redesigned, finally giving Figures 14(g) and 14(h). This is usually a simple procedure, thanks to the help of software tools, e.g., [34]. The final controllers are c_1 in (13) and c_2 in (14).

B. CSTR Mathematical Modelling

Three nonlinear first-order differential equations describe the process behaviour [6]:

(i) The dynamic balance of component A inside the reactor (irreversible exothermic liquid-phase reaction A $\longrightarrow$ B)

$$\frac{dC_a(t)}{dt} = \frac{F(t)}{V_r}\left(C_{a_{\text{in}}}(t) - C_a(t)\right) - k_o e^{-\left(E/R/T_r(t)\right)} C_a(t). \tag{B.1}$$

(ii) The dynamic balance of energy inside the reactor

$$\frac{dT_r(t)}{dt} = \frac{F(t)}{V_r}\left(T_{\text{in}}(t) - T_r(t)\right) - \frac{\lambda}{\rho c_p} k_o e^{-\left(E/R/T_r(t)\right)} C_a(t) - \frac{UA_j}{V_r \rho c_p}\left(T_r(t) - T_j(t)\right). \tag{B.2}$$

(iii) The dynamic balance of energy inside the jacket

$$\frac{dT_j(t)}{dt} = \frac{UA_j}{V_j \rho_j c_{p_j}}\left(T_r(t) - T_j(t)\right) - \frac{F_j(t)}{V_j}\left(T_j(t) - T_{j_{\text{in}}}(t)\right), \tag{B.3}$$

whose parameters are defined in Table 2.

Equilibrium values of main process variables (denoted with subscript "e")

$$\mathbf{q}_j = \left[T_{r_e}, F_e, F_{j_e}, C_{a_{\text{in}_e}}, T_{\text{in}_e}, T_{j_{\text{in}_e}}\right], \tag{B.4}$$

are related by the steady state of the nonlinear differential equations (B.1)–(B.3). Thus, q_j (B.4) denotes an operating point of the system. A particular equilibrium point is adopted as the nominal and denoted with subscript "o" in Table 2.

The nonlinear equations (B.1)–(B.3) are being linearised. The procedure is based on the expansion of the nonlinear function into a Taylor series about the operating point and the retention of only the linear terms.

Then, after taking the Laplace transform, and conveniently substituting and rearranging the equations, a small variation of reactor temperature about equilibrium $\delta T_r(t) = T_r(t) - T_{r_e}$ can be expressed as an s-Laplace function $\Delta T_r(s)$. It depends on two manipulated inputs, the reactant flow $\Delta F(s)$ and the jacket cooling flow $\Delta F_j(s)$; and on three disturbance inputs, the feed concentration $\Delta C_{a_{\text{in}}}(s)$, the inlet temperature $\Delta T_{\text{in}}(s)$, and the inlet coolant temperature $\Delta T_{j_{\text{in}}}(s)$. All these inputs are s-Laplace transforms of $\delta F(t) = F(t) - F_e$, $\delta F_j(t) = F_j(t) - F_{j_e}$, $\delta C_{a_{\text{in}}}(t) = C_{a_{\text{in}}}(t) - C_{a_{\text{in}_e}}$, $\delta T_{\text{in}}(t) = T_{\text{in}}(t) - T_{\text{in}_e}$, and $\delta T_{j_{\text{in}}}(t) = T_{j_{\text{in}}}(t) - T_{j_{\text{in}_e}}$, respectively. Eventually, it yields five 3rd-order output-input transfer functions:

$$m_{j=1,\ldots,5}(s) = \frac{b_{j_2}s^2 + b_{j_1}s + b_{j_0}}{s^3 + a_2 s^2 + a_1 s + a_0}, \quad \text{(B.5)}$$

where $m_1 = (\Delta T_r/\Delta F)$, $m_2 = (\Delta T_r/\Delta F_j)$, $m_3 = (\Delta T_r/\Delta C_{a_{\text{in}}})$, $m_4 = (\Delta T_r/\Delta T_{\text{in}})$, and $m_5 = (\Delta T_r/\Delta T_{j_{\text{in}}})$; coefficients b_{j_k} and a_k ($j = 1, \ldots, 5$; $k = 0, \ldots, 2$) of (B.5) depend on process parameters (Table 2) and equilibrium values in (B.4).

Several operating points (B.4) are being considered as follows: a single equilibrium value is adopted for the controlled variable: $T_{r_e} = T_{r_o}$. The three nonmanipulated inputs are taken as independent variables, whose equilibrium values are estimated as

$$C_{a_{\text{in}_e}} = \{0.9, 1, 1.1\} \times C_{a_{\text{in}_o}}, \quad \text{(B.6)}$$

which represents a variation range of ±10% around nominal $C_{a_{\text{in}_o}}$, and

$$T_{\text{in}_e} = T_{j_{\text{in}_e}} = \{284, 289, 294, 299\}, \quad \text{(B.7)}$$

which represents a variation range of −10/+5 K around nominal T_{in_o}, $T_{j_{\text{in}_o}}$. Finally, the steady state of jacket flow rate is allowed to reach values in-between 65% and 85% of full capacity:

$$F_{j_e} = \{0.65, 0.7, 0.75, 0.85\} \times F_{j_{\max}}. \quad \text{(B.8)}$$

A grid combination of discrete values in (B.6), (B.7), and (B.8) yields 192 cases. Then, the dependent variable F_e for each case is computed from the steady state of the nonlinear differential equations (B.1)–(B.3). Finally, a set of 192 operating points $\mathbf{q}_j$ (B.4) is obtained. Substituting them in the coefficients of (B.5) yields a plant matrix that collects 192 vectors of size 1×5 each one.

Multivariable systems must be conveniently scaled for control design tasks [41]. Here, the presence of a single output makes only necessary to scale the range of the five inputs to the normalized range $[-1, +1]$. The scaling gain for T_{in} is 5, for $T_{j_{\text{in}}}$ is 5, and for $C_{a_{\text{in}}}$ is $0.1C_{a_{\text{in}_o}}$, according to the smallest distance from the nominal equilibrium to the edge value in the variation range. The scaling gain for F_j is $0.2F_{j_{\max}}$ according to the smallest distance from any equilibrium value (B.8) to the maximum flow rate capacity of installation $F_{j_{\max}}$. In a similar way, a scaling gain of $0.29F_{\max}$ for F is computed. These scaling gains are applied to the plants (B.5). Eventually, it is obtained a plant matrix $\mathscr{P}$ that collects 192 vectors $\mathbf{P}(s; \mathbf{q}_j) = [p_1, p_2, p_{d_1}, p_{d_2}, p_{d_3}]$, whose magnitude frequency response is depicted in Figure 6. Let us cite the most relevant information: (i) all p_1-plant cases contain a nonminimum phase zero, which locates over $\omega \in [0.0014, 0.0029]$ rad/s; (ii) all p_2-plant cases have inverse gain; (iii) the maximum resonant pick of the set of plant cases takes place at $\omega = 0.000271$ rad/s and reaches the values 32.2 dB for p_1, 23.5 dB for p_2, 12.1 dB for p_{d_1}, 16.8 dB for p_{d_2}, and 17.1 dB for p_{d_3}.

Data Availability

The data used to support the findings of this study are available from the corresponding author upon request.

Disclosure

The authors are currently at Edificio Departamental - C/San José de Calasanz, 31, 26004 Logroño, La Rioja.

Conflicts of Interest

The authors declare that they have no conflicts of interest.

Acknowledgments

The authors are grateful for the assistance provided by the University of La Rioja.

References

[1] B. J. Allison and S. Ogawa, "Design and tuning of valve position controllers with industrial applications," *Transactions of the Institute of Measurement and Control*, vol. 25, no. 1, pp. 3–16, 2003.

[2] M. A. Henson, B. A. Ogunnaike, and J. S. Schwaber, "Habituating control strategies for process control," *AIChE Journal*, vol. 41, no. 3, pp. 604–618, 1995.

[3] B. Sun, S. Skogestad, J. Lu, and W. Zhang, "Dual SIMC-PI controller design for cascade implement of input resetting control with application," *Industrial & Engineering Chemistry Research*, vol. 57, no. 20, pp. 6947–6955, 2018.

[4] B. J. Allison and A. J. Isaksson, "Design and performance of mid-ranging controllers," *Journal of Process Control*, vol. 8, no. 5-6, pp. 469–474, 1998.

[5] M. Karlsson, O. Slätteke, B. Wittenmark, and S. Stenström, "Reducing moisture transients in the paper-machine drying section with the mid-ranging control technique," *Nordic Pulp & Paper Research Journal*, vol. 20, no. 2, pp. 150–155, 2005.

[6] W. L. Luyben, *Chemical Reactor Design and Control*, Wiley, Hoboken, NJ, USA, 2007.

[7] S. Nájera, M. Gil-Martínez, and J. Rico-Azagra, "Dual-control of autothermal thermophilic aerobic digestion using aeration and solid retention time," *Water (Switzerland)*, vol. 9, no. 6, Article ID 426, 15 pages, 2017.

[8] M. Gil-Martínez, J. Rico-Azagra, and J. Elso, "Frequency domain design of a series structure of robust controllers for multi-input single-output systems," *Mathematical Problems in Engineering*, vol. 2018, Article ID 7531260, 14 pages, 2018.

[9] J. Alvarez-Ramirez, A. Velasco, and G. Fernandez-Anaya, "A note on the stability of habituating process control," *Journal of Process Control*, vol. 14, no. 8, pp. 939–945, 2004.

[10] J. Rico-Azagra, M. Gil-Martínez, and J. Elso, "Quantitative feedback control of multiple input single output systems," *Mathematical Problems in Engineering*, vol. 2014, Article ID 136497, 17 pages, 2014.

[11] S. J. Schroeck, W. C. Messner, and R. J. McNab, "On compensator design for linear time-invariant dual-input single-output systems," *IEEE/ASME Transactions on Mechatronics*, vol. 6, no. 1, pp. 50–57, 2001.

[12] E. Eitelberg, "Some peculiarities of load sharing control," *International Journal of Robust and Nonlinear Control*, vol. 13, no. 7, pp. 607–618, 2003.

[13] M. Garcia-Sanz and F. Y. Hadaegh, "Load-sharing robust control of spacecraft formations: deep space and low Earth elliptic orbits," *IET Control Theory & Applications*, vol. 1, no. 2, pp. 475–484, 2007.

[14] L. Zaccarian, "Dynamic allocation for input redundant control systems," *Automatica*, vol. 45, no. 6, pp. 1431–1438, 2009.

[15] T. A. Johansen and T. I. Fossen, "Control allocation-a survey," *Automatica*, vol. 49, no. 5, pp. 1087–1103, 2013.

[16] R. Mu, X. Zhang, P. Wu, and J. Chen, "RCS and aero surfaces control allocation research on RLV's re-entry phase," *Applied Sciences*, vol. 9, no. 8, 2019.

[17] M. Cocetti, A. Serrani, and L. Zaccarian, "Linear output regulation with dynamic optimization for uncertain linear over-actuated systems," *Automatica*, vol. 97, pp. 214–225, 2018.

[18] O. Johnsson, D. Sahlin, J. Linde, G. Lidén, and T. Hägglund, "A mid-ranging control strategy for non-stationary processes and its application to dissolved oxygen control in a bio-process," *Control Engineering Practice*, vol. 42, pp. 89–94, 2015.

[19] P. A. Luppi, L. Braccia, P. G. Rullo, and D. A. R. Zumoffen, "Plantwide control design based on the control allocation approach," *Industrial & Engineering Chemistry Research*, vol. 57, no. 1, pp. 268–282, 2018.

[20] K. van Heusden, J. M. Ansermino, and G. A. Dumont, "Robust MISO control of propofol-remifentanil anesthesia guided by the NeuroSENSE monitor," *IEEE Transactions on Control Systems Technology*, vol. 26, no. 5, pp. 1758–1770, 2018.

[21] V. Moscardó, P. Herrero, J.-L. Díez et al., "Coordinated dual-hormone artificial pancreas with parallel control structure," *Computers & Chemical Engineering*, vol. 128, pp. 322–328, 2019.

[22] J. Manrique Cordoba, J. Romero Ante, O. Vivas Albán, and J. Sabater Navarro, "Modelo matemático de un paciente con diabetes tipo 1 en lazo cerrado," *Revista Iberoamericana de Automática e Informática industrial*, vol. 7, no. 20, 2019.

[23] Z. Ma, A.-N. Poo, M. H. Ang, G.-S. Hong, and H.-H. See, "Design and control of an end-effector for industrial finishing applications," *Robotics and Computer-Integrated Manufacturing*, vol. 53, pp. 240–253, 2018.

[24] C. Nainer, M. Furci, A. Seuret, L. Zaccarian, and A. Franchi, "Hierarchical control of the over-actuated ROSPO platform via static input allocation," *IFAC-PapersOnLine*, vol. 50, no. 1, pp. 12698–12703, 2017.

[25] U. Schneider, B. r. Olofsson, O. So¨rnmo et al., "Integrated approach to robotic machining with macro/micro-actuation," *Robotics and Computer-Integrated Manufacturing*, vol. 30, no. 6, pp. 636–647, 2014.

[26] T. Haus, A. Ivanovic, M. Car, M. Orsag, and S. Bogdan, "Mid-ranging control concept for a multirotor UAV with moving masses," in *Proceedings of the MED 2018—26th Mediterranean Conference on Control and Automation*, pp. 339–344, Zadar, Croatia, June 2018.

[27] D. Kotarski and J. Kasać, *Chapter Generalized Control Allocation Scheme for Multirotor Type of UAVs, Drones-Applications*, G. Dekoulis, Ed., pp. 43–58, IntechOpen, London, UK, 2018.

[28] S. Jade, J. Larimore, E. Hellstrom, A. G. Stefanopoulou, and L. Jiang, "Controlled load and speed transitions in a multi-cylinder recompression HCCI engine," *IEEE Transactions on Control Systems Technology*, vol. 23, no. 3, pp. 868–881, 2015.

[29] S. Yu, T. K. Chau, T. Fernando, A. V. Savkin, and H. H.-C. Iu, "Novel quasi-decentralized SMC-based frequency and voltage stability enhancement strategies using valve position control and FACTS device," *IEEE Access*, vol. 5, pp. 946–955, 2017.

[30] S. Gayadeen and W. Heath, "An internal model control approach to mid-ranging control," *IFAC Proceedings Volumes*, vol. 42, no. 11, pp. 542–547, 2009.

[31] P. Gorzelic, E. Hellstrom, A. Stefanopoulou, L. Jiang, and S. Gopinath, "A coordinated approach for throttle and wastegate control in turbocharged spark ignition engines," in *Proceedings of the 2012 24th Chinese Control and Decision Conference (CCDC)*, pp. 1524–1529, Taiyuan, China, May 2012.

[32] I. Horowitz, "Survey of quantitative feedback theory (QFT)," *International Journal of Robust and Nonlinear Control*, vol. 11, no. 10, pp. 887–921, 2001.

[33] M. Garcia-Sanz, *Robust Control Engineering: Practical QFT Solutions*, CRC Press, Boca Raton, FL, USA, 2017.

[34] C. Borghesani, Y. Chait, and O. Yaniv, *Quantitative Feedback Theory Toolbox for Use with Matlab*, Terasoft, Hyderabad, India, 2nd edition, 2002.

[35] W.-H. Chen and D. J. Ballance, "QFT design for uncertain non-minimum phase and unstable plants revisited," *International Journal of Control*, vol. 74, no. 9, pp. 957–965, 2001.

[36] M. Sidi, "Feedback synthesis with plant ignorance, non-minimum-phase, and time-domain tolerances," *Automatica*, vol. 12, no. 3, pp. 265–271, 1976.

[37] M. Sidi, "Gain-bandwidth limitations of feedback systems with non-minimum-phase plants," *International Journal of Control*, vol. 67, no. 5, pp. 731–744, 1997.

[38] J. Palacio Morales, J. Isaza Hurtado, A. Tobón Mejía, and J. Herrera Cuartas, "Methodology for NMPC tuning with takagi sugeno fuzzy inference system and multidimensional fuzzy sets for applications in non-linear chemical processes," *Revista Iberoamericana de Automática e Informática Industrial*, vol. 16, pp. 100–113, 2019.

[39] L. Torralba-Morales, G. Reynoso Meza, and J. Carrillo-Ahumada, "Sintonización y comparación de conceptos de diseño aplicando la optimalidad de Pareto. Un caso de estudio del biorreactor de Cholette," *Revista Iberoamericana de Automática e Informática industrial*, vol. 12, no. 2, 2019.

[40] F. G. Shinskey, "Control systems can save energy," *Chemical Engineering Progress*, vol. 74, pp. 43–46, 1978.

[41] S. Skogestad and I. Postlethwaite, *Multivariable Feedback Control. Analysis and Design*, John Wiley & Sons, Chichester, England, 2005.